Fizika Nizkikh Temperatur, 2002, v. 28, No. 3, p. 288–296

Raman scattering in $LiNiPO_4$ single crystal

V. I. Fomin, V. P. Gnezdilov, V. S. Kurnosov,
A. V. Peschanskii, and A. V. Yeremenko

B. Verkin Institute for Low Temperature Physics and Engineering of the National Academy of Sciences of Ukraine, 47 Lenin Ave., 61103, Kharkov, Ukraine
E-mail: gnezdilov@ilt.kharkov.ua

H. Schmid, J.-P. Rivera, and S. Gentil*

Department of Inorganic, Analytical and Applied Chemistry, University of Geneva CH-1211 Geneva 4, Switzerland

Received November 1, 2001

The complete Raman spectra of a single crystal of $LiNiPO_4$ for a wide temperature range are reported. Among the 36 Raman-active modes predicted by group theory, 33 have been detected. The analysis of the spectra in terms of internal modes of the $(PO_4)^{3-}$ group and of external modes is done with success. Besides, the multiphonon Raman scattering is discussed. Low-frequency lines, observed in the antiferromagnetic phase, are assigned to magnon scattering and are discussed briefly.

PACS: 78.30.Hv

Introduction

The lithium orthophosphate of nickel belongs to a family of antiferromagnets with the general formula $LiMPO_4$ (where M = Fe^{2+}, Mn^{2+}, Co^{2+}, Ni^{2+}) and which are known to be magnetoelectrics [1,2]. In the paramagnetic phase these compounds have the same orthorhombic space group *Pnma*, but the magnetic groups in their antiferromagnetic phase are partly different. All of them allow the occurrence of the linear magnetoelectric (ME) effect. The mechanisms responsible for the ME effect in $LiMPO_4$ remain an open question.

The majority of experimental investigations of the linear ME effect in $LiMPO_4$ compounds realized so far have been restricted to the study of the quasistatic properties, i.e., to measurement of the quasistatic magnetic (electric) moment induced by an external quasistatic electric (magnetic) field. Much less attention has been paid to the spectrum of elementary excitations and to the influence of ME interaction on excited states. The nature of the large value of the ME coefficient in $LiCoPO_4$ is not yet clear. It may lie in the specific arrangement of the low-energy electronic energy levels of the magnetic ion and their interaction with a vibrational spectrum.

The motivation for the present study is manifold. One of the objectives is to determine the frequency and symmetry of the long-wavelength, or $\mathbf{k} = 0$, Raman-active phonons and to compare them with the results of group theory analysis, based both on the factor group and site symmetry methods.

At low temperature $LiNiPO_4$ undergoes a transition to an antiferromagnetic (AF) phase, and thus additional lines in consequence of the light scattering by spin waves, both first and second order, may be observed in the Raman spectra.

Owing to the ME effect the Raman spectrum may be more complicated in the AF phase due to an additional mechanism of light scattering predicted by Pradhan [3]. The origin of the mechanism resides in the possibility (via ME) interaction of the electrical (magnetic) vector of the incident light

* New address: Swiss Federal Institute of Technology Lausanne, Materials Department, Laboratory of Ceramics, CH-1015 Lausanne, Switzerland.

with the magnetic (electric) vector of the scattered light. The effect should be proportional at least to the value of the ME coefficients at the frequency of visible light, which are unknown. The «Pradhan» lines in the spectrum may in principle be separated via their difference given by the polarization selection rules.

Motivated by the above considerations, a Raman scattering study of $LiNiPO_4$ has been undertaken. In this paper we are reporting spectra of the observed elementary excitations in the frequency region from 4 to 1200 cm^{-1} and at temperatures between 5 and 300 K.

Synthesis of $LiNiPO_4$ single crystals and experimental procedure

Single crystals of the orthophosphates $LiMPO_4$ (M = Mn, Fe, Co, Ni) can be obtained by conventional solution growth (see, e.g., [4] and [5]) in LiCl flux. This high-temperature halide solvent is advantageous as it consists partially of an element present in the final compound and has rather low viscosity in the molten phase, favoring stable growth. Different experimental variants according to the following reactions are possible for obtaining the starting orthophosphate:

$$M(OH)_2 + NH_4H_2PO_4 + Li_3PO_4 \rightarrow LiMPO_4 + NH_3 + H_2O\ , \quad (1)$$

$$M_3(PO_4)_2 + Li_3PO_4 \rightarrow 3\ LiMPO_4\ , \quad (2)$$

$$MCl_2 + Li_3PO_4 \rightarrow LiMPO_4 + 2\ LiCl\ . \quad (3)$$

For each of these reactions, a stoichiometric molar ratio of reacting materials is required. Reaction (2) was first used for the synthesis of $LiMnPO_4$ crystals by dissolving the starting reactants in LiCl, followed by cooling [6]. The method was later modified slightly for the growth of $LiFePO_4$ crystals [7] and adapted for the growth of single crystals of the entire series $LiMPO_4$, with M = Mn, Fe, Co and Ni [8].

In the present study, for growing $LiNiPO_4$ single crystals, reaction (3) was used and performed in a LiCl flux, allowing us to obtain single crystals large enough for physical experiments (~ 1–5 mm^3). The molar ratio between $LiNiPO_4$ and LiCl in the starting mixture was optimized at 1:3. Platinum crucibles of 30 ml volume were filled with a maximum of 45 g of a stoichiometric mixture of the powders, followed by a pre-melting at 800 °C. Due to the high volatility of the solvent, the crucibles were sealed by argon arc welding and a hole of ~ 50 μm diameter was drilled through the lid in order to equilibrate the pressure.

The growth temperature profile was as follows: 1) heating in 5 h to 890 °C, 2) soaking at 890 °C for 4 h, 3) slow-cooling at 0.755 °C/h to 715 °C, 4) slow-cooling at 1.4 °C/h to 680 °C and 5) crystal recovery at 680 °C. The crystal recovery from the molten flux was the last critical problem to be solved for obtaining weakly stressed crystals. For this purpose the crucible was rapidly removed from the furnace, two holes were pierced in the lid, and the remaining liquid was quickly poured on a porous ceramic.

The Raman spectra were measured on a $LiNiPO_4$ single crystal of high optical quality. The sample was cut as a rectangular parallelepiped with edges of 4.2, 3.0, and 2.4 mm length, parallel to the crystallographic axes a, b, c of the orthorhombic cell, respectively. Since the a, b, and c axes correspond to the principal axes of the dielectric tensor, this sample shape minimized errors due to birefringence in polarized Raman measurements. The system of coordinates was chosen to be $X \parallel a$, $Y \parallel b$ and $Z \parallel c$.

The Raman spectra were recorded with a Jobin-Yvon U-1000 double monochromator equipped with a cooled photomultiplier and photon counting electronics. The right-angle scattering geometry was used. In order to reduce the beam-induced heating of the sample and to enhance the scattered light intensity, the 632.8 nm line of a He–Ne laser operating at powers up to 30 mW, was used in the experiments. For the yellow-orange crystals of $LiNiPO_4$, the transmission window is centered in the region of ~ 573 nm [9,10]. The temperature interval 4.2–300 K was covered by using a special optical cryostat. The sample was kept in an exchange gas atmosphere.

Structural and magnetic features of $LiNiPO_4$

The lithium orthophosphates $LiMPO_4$ (M = = Co^{2+} or Ni^{2+}) are isostructural with the minerals lithiophilite (M = Mn) and triphilite (M = Fe), which belong to the olivine family [1,11,12]. The orthorhombic unit cell contains four formula units and is described by space group *Pnma* (D_{2h}^{16}) [12]. The crystal structure can be understood as a nearly hexagonal close packing of oxygen atoms. Each phosphorus atom in the crystal is surrounded by four oxygen atoms, creating a distorted tetrahedral $(PO_4)^{3-}$ group with C_s ($m \perp b$) point symmetry. The

Ni^{2+} and Li^{2+} ions occupy the positions with site symmetry C_s and C_i, respectively. They are surrounded by distorted octahedra of oxygen atoms. Nickel ions lie in puckered planes perpendicular to the a axis. Adjacent planes are separated by PO_4 tetrahedra sharing corners and edges with the LiO_6 octahedra.

Above $T_N = 19.1$ K the crystal manifests paramagnetic behavior [13]. Below T_N a relatively strong AF coupling between nearest-neighbor nickel ions is occurring within the puckered plane via –Ni–O–Ni– superexchange pathways [11,13,14]. However, there is no direct or first-order superexchange (via one common ion) coupling between the moments in different planes, and only higher-order interactions are possible, involving the phosphate groups as an «exchange bridge». Each Ni^{2+} has a net of at least four antiferromagnetic –Ni–O–P–O–Ni– links to Ni^{2+} ions in adjacent planes. According to neutron scattering data [13,14], the antiferromagnetic ordering takes place with preservation of the unit cell. The spins of the nickel ions lie along the crystal axis c and alternate up and down. Up to now the magnetic space and point groups were considered to be $Pnm'a$ and $mm'm$, respectively [11]. Recent neutron diffraction work has shown that a space-modulated spin structure occurs in a narrow temperature range close to T_N with a magnetic incommensurate short range order persisting up to about 40 K [15,16].

The magnetic field dependence of the polarization induced via the ME effect in $LiNiPO_4$ shows a so-called «butterfly loop» feature both for the magnetic field H applied along the a axis, i.e. perpendicular to the spin direction (c axis) [17], as well as for H applied along the spin direction [18]. Usually such behavior appears due to the presence of a spontaneous magnetic moment in a compound (see, e.g., [19,20]). Since such a small spontaneous magnetization was recently found for the related $LiCoPO_4$ [21], also showing «butterfly loops» [2], the occurrence of a spontaneous magnetization in $LiNiPO_4$ can be expected, too. Thus a symmetry lower than $mm'm$ will be required.

In spite of the fact that the $mm'm$ symmetry forbids a spontaneous magnetic moment, it was recently shown theoretically that a «butterfly loop» can also be realized in 4-sublattice fully compensated antiferromagnets with an «indirect cross» magnetic structure [22]. In such a structure the above-mentioned symmetry $mm'm$ allows spin canting in the pairs of adjacent sublattices, but the resulting magnetic moment of a pair is «hidden», because another spin pair fully compensates it in the unit cell. However, this mechanism does not seem to apply to $LiNiPO_4$ because, as stated above, it is very likely that the «butterfly loops» are due to a spontaneous magnetization.

Group theory analysis of fundamental vibrations

The group theory analysis of the $LiMPO_4$ family compounds has been done in [23]. Let us summarize the essential results. In all of them the unit cell contains 4 formula units. The vibrational representation $\Gamma_{\rm vibr}$ of the 84 normal modes at the center of the Brillouin zone ($\mathbf{k} = 0$) is distributed on the irreducible representations of the D_{2h} point group as follows: $\Gamma_{\rm vibr} = 11A_g + 7B_{1g} + 11B_{2g} + 7B_{3g} + 10A_u + 14B_{1u} + 10B_{2u} + 14B_{3u}$. Among them there are 3 acoustic modes, 45 antisymmetrical modes, active in IR absorption for the B_{1u}, B_{2u}, and B_{3u} representations, and 36 symmetrical Raman-active optical modes. The latter modes correspond to the polarization of the excited and scattered light in the chosen coordinate system as: A_g–(XX), (YY), (ZZ), B_{1g}–(XY), (YX), B_{2g}–(XZ), (ZX), and B_{3g}–(YZ), (ZY).

In a first-order approximation, the vibrations can be separated into internal vibrations ($\Gamma_{\rm int}$) of the $(PO_4)^{3-}$ tetrahedra and external vibrations in which they move and rotate as solid units. The external vibrations are separated into the translational motions of the center of mass of $(PO_4)^{3-}$, Li^+ and Co^{2+} ions ($\Gamma_{\rm trans}$) and hindered rotations (librations) of the $(PO_4)^{3-}$ ions ($\Gamma_{\rm libr}$). Such separation is rather arbitrary and may be used in the group-theory analysis for clarity only. In fact, they are not completely independent. The analysis gives the following representation for the above-listed types of vibration:

$$\Gamma_{\rm int} = 6A_g + 3B_{1g} + 6B_{2g} + 3B_{3g} + 3A_u + 6B_{1u} + 3B_{2u} + 6B_{3u}\,,$$

$$\Gamma_{\rm trans} = 4A_g + 2B_{1g} + 4B_{2g} + 2B_{3g} + 5A_u + 6B_{1u} + 4B_{2u} + 6B_{3u}\,,$$

and

$$\Gamma_{\rm libr} = A_g + 2B_{1g} + B_{2g} + 2B_{3g} + 2A_u + B_{1u} + 2B_{2u} + B_{3u}\,.$$

Theoretically, a static splitting due to the C_s crystal field symmetry and a dynamic splitting due to the presence of 4 formula units in the unit cell could take place for the frequencies of the internal vibrations of $(PO_4)^{3-}$ tetrahedra. Experimentally, this may or may not be observed, depending on the crystal field effects.

Experimental results and discussion

Polarized Raman spectra of a $LiNiPO_4$ single crystal, taken at 5 K for different orientations of the sample sufficient to classify the symmetry types of all the Raman-active modes, are shown in Fig. 1. The intense lines which persist when the temperature rises from $T < T_N$ to room temperature are identified here as first-order phonon excitations. The symmetry assignments were made by means of polarization measurements and are listed in Table. Some «leak through» of forbidden lines in certain polarization configurations is evident in these spectra, arising from slight disorientation of the crystal and/or the wide angle aperture optics which is used in the experiments to collect scattered light. The Raman spectra of $LiNiPO_4$ are very similar to those of $LiCoPO_4$ [23].

Study of internal modes

Characteristic phonon lines with frequencies higher than 400 cm^{-1} are observed. The lines were identified in accordance with their closeness to the frequencies of the fundamental vibrational modes of a free PO_4 tetrahedron, which are 980 (ν_1), 365 (ν_2), 1082 (ν_3), and 515 (ν_4) cm^{-1} [24]. The reducible vibrational representation of a free PO_4 tetrahedron decomposes to $A_1 + E + F_1 + 3F_2$ irreducible representations of its T_d symmetry group. The internal modes are labeled using Herzberg's notation [24] as: ν_1 (A_1, symmetric P–O stretching), the doubly degenerate ν_2 (E, symmetric O–P–O bond bending), the triply degenerate ν_3 (F_2, antisymmetric P–O stretching), and the triply degenerate ν_4 (F_2, antisymmetric O–P–O bond bending). The remaining modes F_1 and F_2 are external and correspond to rotation and translation of PO_4 as a whole unit, respectively.

In $LiNiPO_4$ the point symmetry of $(PO_4)^{3-}$ ions is C_s, which is lower than the T_d symmetry of the free ion, hence the degeneracy of the free ion frequencies must be lifted as: $A_1 \to A'$, $E \to A' + A''$, $F_1 \to A' + 2A''$, $F_2 \to 2A' + A''$. Since there are four $(PO_4)^{3-}$ ions within the primitive unit cell, there are four times as many modes of each species. They can be further related to the D_{2h} factor group symmetry of the crystal giving the rules:

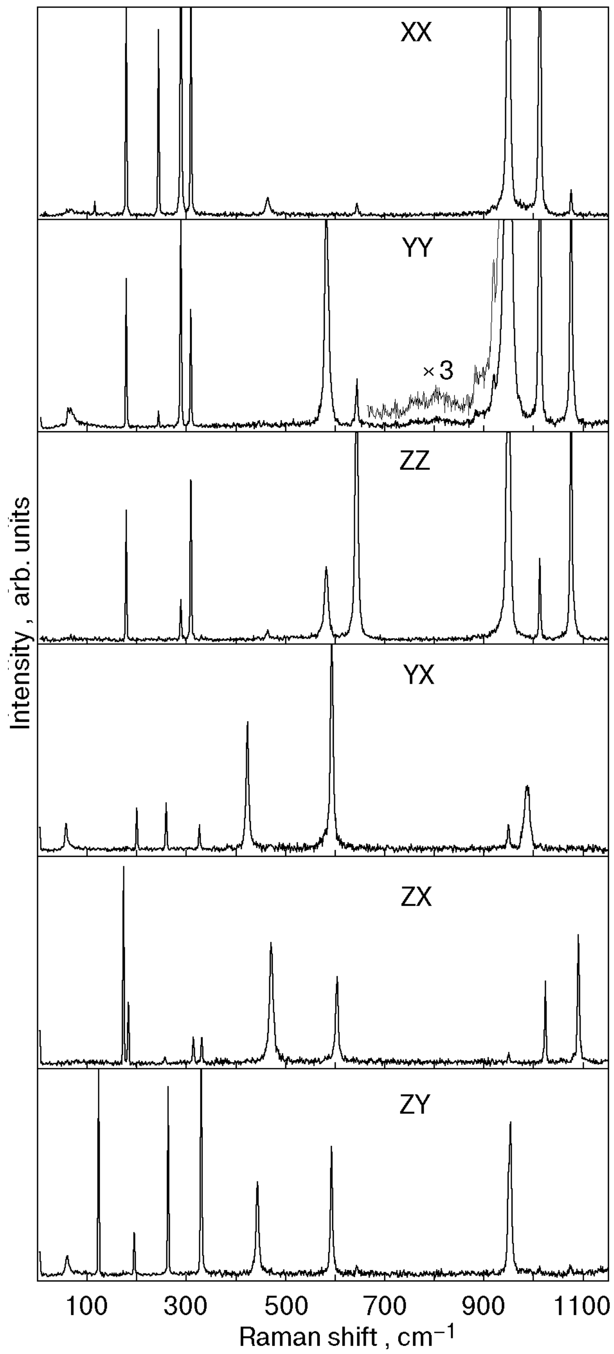

Fig. 1. Low-temperature (5 K) polarized Raman spectra of a $LiNiPO_4$ single crystal. The spectral resolution is 2.0 cm^{-1}.

$4A' \to A_g + B_{2g} + B_{1u} + B_{3u}$ and $4A'' \to B_{1g} + B_{3g} + A_u + B_{2u}$. As a result, the internal phonons at $\mathbf{k} = 0$ in the $LiNiPO_4$ crystal originate from the fundamental vibrational modes of a free PO_4 tetrahedron as shown in the following scheme: $\nu_1 \to A_g + B_{2g} + B_{1u} + B_{3u}$, $\nu_2 \to A_g + B_{1g} + B_{2g} + B_{3g} + A_u + B_{1u} + B_{2u} + B_{3u}$, ν_3 and $\nu_4 \to 2A_g + B_{1g} + 2B_{2g} + B_{3g} + A_u + 2B_{1u} + B_{2u} + 2B_{3u}$. The frequencies of the phonons may be split due to a dynamical effect.

Table

Experimentally observed frequencies (cm^{-1}) of vibrational excitations of the $LiNiPO_4$ single crystal at 5 K (300 K) and their classification

Type of vibrations		Symmetry of vibrations A_g	B_{1g}	B_{2g}	B_{3g}
External		114.0 (111.5)			
					122.0 (119.5)
			–		
				172.0 (170.0)	
		175.5 (175.0)			
				182.0 (181.5)	
					193.5 (189.0)
			199.0 (195.0)		
		242.5 (238.0)			
				255.5 (252.0)	
			258.0 (256.0)		
					262.0 (258.5)
		287.5 (282.5)			
		308.0 (303.5)			
				313.0 (310.0)	
			325.0 (320.5)		
					329.0 (324.5)
				329.5 (325.5)	
Internal PO_4	$E(\nu_2)^*$		422.5 (417.5)		
					442.5 (437.0)
		462.5 (459.0)			
				470.5 (467.5)	
	$F_2(\nu_4)^*$	581.5 (580.0)			
					592.0 (591.0)
			592.5 (591.5)		
				603.0 (601.0)	
		642.0 (640.0)			
				–	
	$A_1(\nu_1)^*$	948.5 (948.5)			
				–	
	$F_2(\nu_3)^*$				953.0 (952.0)
			986.0 (987.5)		
		1011.5 (1010.5)			
				1023.0 (1022.5)	
		1074.5 (1072.0)			
				1090.0 (1088.0)	

* Irreducible representations and the internal mode indexes of a free PO_4 tetrahedron [24].

In the crystal, the value of frequency splitting of the ν_i (i = 1–4) modes of the phosphate group is an indicator of the strength of the coupling to an environment. In the absence of interaction between them, the modes in quartets $A_g + B_{2g} + B_{1u} + B_{3u}$ and $B_{1g} + B_{3g} + A_u + B_{2u}$, which originate from A' and A'' types of vibrations respectively, would each have the same frequency. Unfortunately, to the best of the authors' knowledge, no IR work has yet been done for this single crystal*. Hence we

* The only published data [25] concern IR spectra of polycrystalline samples of $Li_{1-3x}Fe_xNiPO_4$ ($0 < x < 0.15$).

have no experimental data about IR-active phonons with B_{1u} , B_{3u} , and B_{2u} symmetry (A_u phonons are neither IR nor Raman active), which belong to the above-mentioned quartets, and so we have no possibility to calculate the full range of frequency splitting of the ν_i modes in the crystal. Nevertheless, the frequency separation of A_g and B_{2g} , and of B_{1g} and B_{3g} modes indicate that dynamical effects are far from negligible (see Table). It should be noted that the B_{2g} component of the stretching mode ν_1 is weak and difficult to observe.

The separation of fundamental vibrations into internal and external ones is valid in the case where the respective vibration frequencies differ considerably. Although the lowest Raman-active internal modes at ~ 420 cm^{-1} are quite far from the highest external modes at ~ 330 cm^{-1}, the situation is not so clear for antisymmetrical modes. For example, the external antisymmetrical vibrations which involve translational motions of light Li^+ ions, are expected to be higher in frequency. Nevertheless, the internal–external modes approximation still retains the merit of providing a good basis for understanding of $\mathbf{k} = 0$ modes in the $LiMPO_4$ compound.

Study of external modes

Following the scheme given above, all sharp lines below 330 cm^{-1} and above 100 cm^{-1} are assigned to the external librational and translational modes. An essential difference between the XX, YY, and ZZ diagonal components of the scattering tensor, belonging to A_g symmetry, reflects the considerable anisotropy of the $LiNiPO_4$ structure (Fig. 1). It is evident from Table that the correct number of bands with A_g , B_{2g} , and B_{3g} symmetry is present, while the number of B_{1g} peaks is deficient. Only 3 peaks are clearly visible in the spectra of appropriate polarization. Since the crystal undergoes no structural phase transitions, the phonon lines show only a weak frequency shift and broadening with increasing temperature. The total shift of all phonon lines in the temperature range from 4.2 to 300 K does not exceed 5 cm^{-1} (Table).

An assignment of these lines to rotational and translational modes is conditional, because they have the same symmetry and, hence, may strongly interact with one another. We can only say something about the specific contribution of rotation and translation in each real mode in the crystal. It is known [26] that the temperature dependence of the phonon linewidth is determined mainly via two mechanisms: (i) unharmonicity of the corresponding vibrational mode and (ii) relaxation processes which may be related to many-particle decay or accidental reorientation, typical for atomic complexes. The first mechanism provides a linear temperature dependence of the spectral linewidth, while the second one is represented as Arrhenius-like contribution to the line broadening.

The reorientational motions in the $LiMPO_4$ crystals can be accomplished by the $(PO_4)^{3-}$ tetrahedra only during their hindered rotations. Hence the B_{3g} modes at 174.5 and 323 cm^{-1} in the $LiCoPO_4$ have been preferentially assigned to librations [23], due to the essential contribution of the mechanism (ii) to the temperature dependence of their widths. It is interesting that only the B_{3g} spectrum shows an essential difference in the character of line broadening (Fig. 2). In the frequency range of external vibrations the B_{3g} spectrum contains 2 translational and 2 librational modes. The first pair may be described as translational motions of the Ni^{2+} ions relative to the $(PO_4)^{3-}$ ions parallel to the crystal axis b. The second one is represented by linear combinations of in-phase, around axis a, and out-of-phase, around axis c, rotations of four $(PO_4)^{3-}$ tetrahedra in the unit cell. The experimental results for the temperature dependence of the damping of the corresponding B_{3g} modes at 193 and 329 cm^{-1} in $LiNiPO_4$ are found to be similar to $LiCoPO_4$ (Fig. 3). This supports our assignment of these modes to ones of predominantly rotational

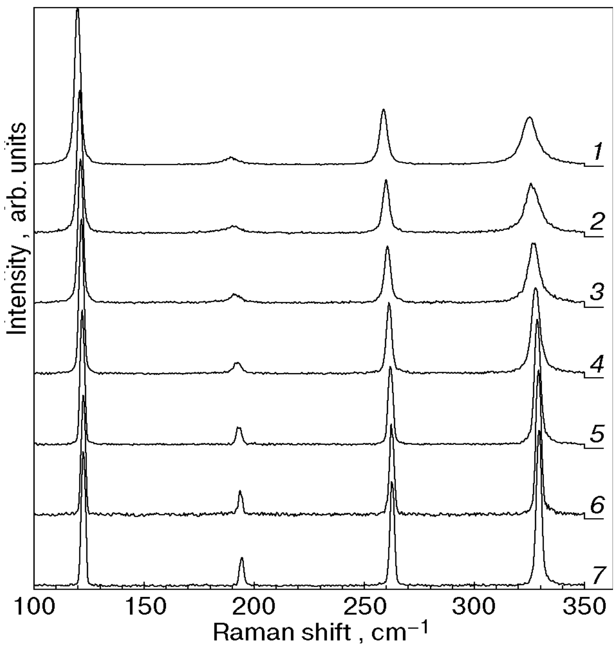

Fig. 2. Temperature behavior of the B_{3g} external modes in $LiNiPO_4$. The numbers indicate the temperature in K: 300 (*1*), 250 (*2*), 200 (*3*), 150 (*4*), 90 (*5*), 25 (*6*), 5 (*7*). The spectral resolution is 2.0 cm^{-1}.

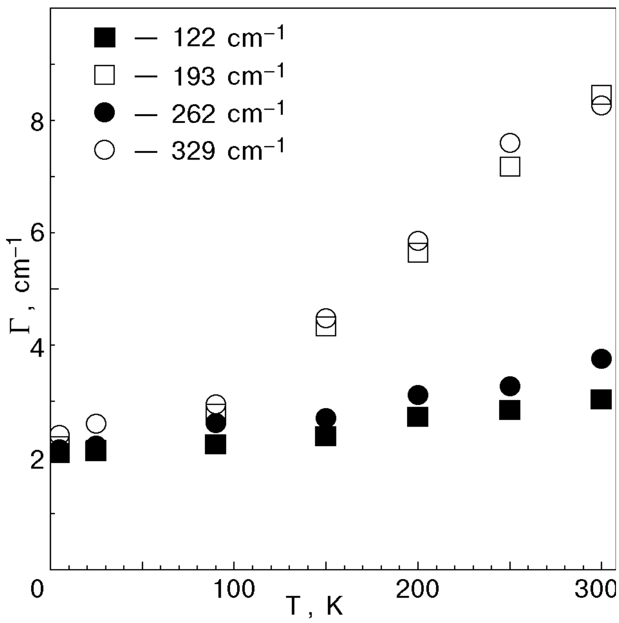

Fig. 3. Temperature dependence of the width Γ at half the height of the phonon lines in the low-frequency B_{3g} spectrum (see Fig. 2).

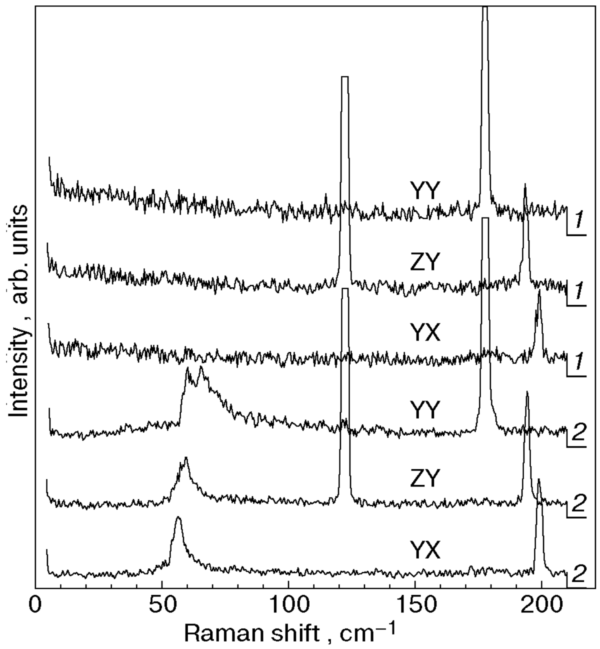

Fig. 4. Low-frequency spectra of $LiNiPO_4$ at 25 (*1*) and 5 (*2*) K. The sharp lines at 122, 177.5, 193.5, and 199 cm^{-1} are the vibrational modes. The spectral resolution is 2.0 cm^{-1}.

character. In the other polarizations the temperature behavior of linewidths does not show enough difference to give priority to one of the two mechanisms of broadening. Thus the classification of the external modes remains, of course, qualitative.

Second order vibrational spectra

In addition to one-phonon peaks, there are weak features around 750, 811, 887, and 919 cm^{-1} in the polarizations corresponding to the diagonal components of the scattering tensor, which we assign to two-phonon scattering (see Fig. 1). A more prominent structure is evident in YY polarization. In the off-diagonal Raman polarizations the second-order spectrum is weak.

The bands at 887 and 919 cm^{-1} can be assigned to the two-phonon excitation and overtone of 442.5 and 462.5 cm^{-1} bending modes, respectively. Of course they can also be formed by combination of other modes with approximately correct frequencies, such as: (581.5 + 308), (592.5 + 325), and (582 + 329) cm^{-1}.

The broad bands at 750 and 811 cm^{-1} are very likely the combination of O–P–O bond bending vibrations ν_2 and ν_4 and some external modes, for example: (462+287.5), (581.5+242.5), (422.5+325), (470.5 + 329.5), (442.5 + 329) cm^{-1}. In contrast to overtones the combined bands arise from two-particle processes, which involve pairs of phonons with the only restriction that the sum wave vector must be zero. If phonons in the pair have some frequency dispersion, they produce broad bands in a second-order Raman spectrum.

Low-frequency excitations in AF phase

In the low-frequency Raman spectra of $LiNiPO_4$ a set of lines appears at $T < T_N$. Representative spectra in three experimental geometries, recorded at temperatures above and below T_N and covering the frequency range 0–210 cm^{-1}, are shown in Fig. 4. Well below T_N the YY spectrum comprises a peak at 60 cm^{-1}, accompanied by a broad asymmetric band which shows a maximum intensity at 66.5 cm^{-1}, and the cutoff frequency is about 130 cm^{-1}. There is a peak at 58.5 cm^{-1} in the ZY spectrum and a peak at 56.5 cm^{-1} with a shoulder on the low-frequency side of the YX spectrum. No visible features were observed in the XZ spectrum, and so it is not reproduced here. The observed peaks are attributed to magnon scattering, because they vanish above T_N = 19.1 K. However, a definite assignment of the lines to distinct excitations modes is not possible at the present stage of investigation. There are no data on the magnon dispersion curves nor results of antiferromagnetic resonance experiments from which the energy of a zone-center (**k** = 0) magnon at T = 0 K may be estimated. For the time being we can only note that the number of observed lines in the Raman spectra of $LiNiPO_4$ at $T << T_N$ exceeds the number that may be predicted by the square two-dimensional model of the antiferromagnet used in [13].

Conclusion

Finally, we summarize the present results and the remaining problems. The Raman spectrum of $LiNiPO_4$ displays reasonable agreement with group theory predictions. The internal–external modes approximation is satisfactory for the lattice dynamics of $LiMPO_4$ compounds. The vibrations of the $(PO_4)^{3-}$ ions may be treated by the site group method. The observed splitting of the ν_2 , ν_3 , and ν_4 modes of the «free» tetrahedral complex indicate that in $LiNiPO_4$ the host-lattice phosphate interaction and the dynamic coupling between $(PO_4)^{3-}$ complexes is not weak.

Due to the anharmonicity of the vibrational modes, overtones, and two-phonon excitations, which are combinations of the external and the bending vibrations of the $(PO_4)^{3-}$ complexes, are observed in the Raman spectra.

We have revealed no violations of the polarization selection rules below the Néel temperature of $LiNiPO_4$ which may be connected with the Pradhan mechanism of light scattering in ME crystals [3]. Thus the effect is considered to be weak [1] and hence it will be difficult to observe it in this compound. The static values of the ME susceptibility in $LiNiPO_4$ are considerably smaller than in $LiCoPO_4$, as experiments [2] have shown. By assuming that the magnetoelectric coefficients are not much changed at optical frequencies from their static values, there is a chance to observe them in $LiCoPO_4$. In addition, detailed investigations of phonons by infrared absorption are necessary. To the best of the authors' knowledge, no IR work has yet been done on these single crystals, and such experiments would be very helpful in the discussion of this new effect in Raman scattering.

The evidence of long-range antiferromagnetic order is observed in the form of the appearance of additional lines at 56.5, 58.5, 60 cm^{-1} and of a broad asymmetric band at 66.5 cm^{-1} at temperatures below T_N . Their frequencies and behavior with changing temperature allow them to be identified as the Raman scattering on spin-wave excitations. A definite assignment of the lines to distinct excitations is not possible at the present stage of investigation. Detailed experimental data on the temperature and magnetic field dependence of the low-frequency Raman spectrum of $LiNiPO_4$ remain a topic for future study.

Acknowledgments

The authors thank Prof. N. F. Kharchenko for helpful discussions and steady interest in the work.

1. M. Mercier, J. Gareyte, and E. F. Bertaut, *C. R. Acad. Sc. Paris* **B264**, 979 (1967).
2. J.-P. Rivera, *Ferroelectrics* **161**, 147 (1994).
3. T. Pradhan, *Phys. Scripta* **45**, 86 (1992).
4. H. J. Scheel and D. Elwell, *Crystal Growth from High-Temperature Solutions*, Academic Press, London (1975).
5. W. Tolksdorf, in: *Handbook of Crystal Growth. Vol. 2: Bulk Crystal Growth*, D. T. J. Hurle (ed.), North-Holland Elsevier Science Publishers, Amsterdam (1994), Part 2a, Chapt. 10, p. 563.
6. F. Zambonini and L. Malossi, *Z. Kristallogr.* **80**, 442 (1931).
7. R. E. Newnham, R. P. Santoro, and M. J. Redman, *J. Phys. Chem. Solids* **26**, 445 (1965).
8. M. Mercier, *These de doctorat d'Etat*, Faculte des Sciences, Universite de Grenoble, France (1969).
9. G. E. Rossman, R. D. Shannon, and R. K. Waring, *J. Solid State Chem.* **39**, 277 (1981).
10. A. Belletti, R. Borromei, R. Cammi, and E. Cavalli, *Phys. Status Solidi* **B163**, 281 (1991).
11. R. P. Santoro, D. J. Segal, and R. E. Newnham, *J. Phys. Chem. Solids* **27**, 1192 (1966).
12. I. Abrahams and K. S. Easson, *Acta Crystallogr.* **C49**, 925 (1993).
13. D. Vaknin, J. L. Zarestky, J. E. Ostenson, B. C. Chakoumakos, A. Goni, P. J. Pagliuso, T. Rojo, and G. E. Barberis, *Phys. Rev.* **B60**, 1100 (1999).
14. R. P. Santoro, R. E. Newnham, and S. Nomura, *J. Phys. Chem. Solids* **27**, 655 (1966).
15. D. Vaknin and J. L. Zarestky, *Abstract [24.006]*, in: *The 2000 March Meeting of the American Physical Society*, Minneapolis, March 23, 2000.
16. D. Vaknin et al., *to be published*.
17. I. Kornev, M. Bichurin, J.-P. Rivera, S. Gentil, H. Schmid, A. G. M. Jansen, and P. Wider, *Phys. Rev.* **B62**, 12247 (2000).
18. I. Kornev et al., *to be published*.
19. E. Ascher, H. Rieder, H. Schmid, and H. Stossel, *J. Appl. Phys.* **37**, 1404 (1966).
20. M. Senthil Kumar, J.-P. Rivera, Z. G. Ye, S. D. Gentil, and H. Schmid, *Ferroelectrics* **204**, 57 (1997).
21. N. F. Kharchenko, Yu. N. Kharchenko, R. Szymchak, M. Baran, and H. Schmid, *Fiz. Nizk. Temp.* **27**, 1208 (2001) [*Low Temp. Phys.* **27**, 895 (2001)].
22. I. E. Chupis, *Fiz. Nizk. Temp.* **26**, 574 (2000) [*Low Temp. Phys.* **26**, 422 (2000)].
23. V. I. Fomin, V. P. Gnezdilov, V. S. Kurnosov, A. V. Peschanskii, V. V. Eremenko, S. Gentil, and J.-P. Rivera, *Fiz. Nizk. Temp.* **25**, 1107 (1999) [*Low. Temp. Phys.* **25**, 829 (1999)].

24. G. Herzberg, *Infrared and Raman Spectra of Polyatomic Molecules*, Van Nostrand, New York (1975).
25. A. Goni, L. Lezama, M. I. Arriortua, G. E. Barberis, and T. Rojo, *J. Mater. Chem.* **10**, 423 (2000).
26. M. M. Suschinsky, *Raman Scattering Spectra of Molecules and Crystals*, Nauka, Moscow (1969) (in Russian).